Wrench-Closure Workspace Generation for Cable Driven Parallel Manipulators using a Hybrid Analytical-Numerical Approach

Darwin Lau
Department of Mechanical Engineering
the University of Melbourne
Melbourne, Australia

Denny Oetomo
Department of Mechanical Engineering
the University of Melbourne
Melbourne, Australia
Email: doetomo@unimelb.edu.au

Saman Halgamuge
Department of Mechanical Engineering
the University of Melbourne
Melbourne, Australia
Email: saman@unimelb.edu.au

ABSTRACT

In this paper, a technique to generate the wrench-closure workspace for general case completely restrained cable driven parallel mechanisms is proposed. Existing methods can be classified as either numerically or analytically based approaches. Numerical techniques exhaustively sample the task space, which can be inaccurate due to discretisation and is computationally expensive. In comparison, analytical formulations have higher accuracy, but often provides only qualitative workspace information. The proposed hybrid approach combines the high accuracy of the analytical approach and the algorithmic versatility of the numerical approach. Additionally, this is achieved with significantly lower computational costs compared to numerical methods. It is shown that the wrench-closure workspace can be reduced to a set of univariate polynomial inequalities with respect to a single variable of the end-effector motion. In this form, the workspace can then be efficiently determined and quantitatively evaluated. The proposed technique is described for a 3-DOF and a 6-DOF cable driven parallel manipulator. A detailed example in workspace determination using the proposed approach and comparison against the conventional numerical approach are presented.

1 Introduction

Cable driven parallel manipulators are structurally similar to traditional parallel mechanisms, but differ in that rigid links are replaced by cables. The manipulator's movement is regulated through the actuation of the individual cables that are attached to the end effector on one end and to the actuator located at the base platform on the other. This class of manipulator has been widely studied due to its desirable characteristics over traditional parallel mechanisms: reduced weight and inertia, simplified dynamics modelling, ease of transportation and construction, and ease of reconfigurability.

The use of lightweight cables with negligible inertia simplifies the dynamics, modelling and control of the system. In addition, cable mounting points at the base platform can be relocated to result in a highly reconfigurable and resizable workspace. With these advantages, a range of applications exist for cable driven robots [1], such as manipulation of heavy payloads for manufacturing [2] [3] and cargo handling [4], interaction and sensing with the environment [5] [6], aerial camera, haptics [7] and building construction [8]. Applications in the medical field include rehabilitation [9] [10] and exoskeletons [11] [12].

Knowledge of the end effector's usable workspace is essential for several purposes, such as trajectory planning [13], and the selection and design of manipulator configurations depending on workspace requirements [14]. The configuration of a cable driven manipulator refers to the location of cable attachments at the base platform and the end effector. A unique property of cable driven mechanisms is that cables can only be actuated unilaterally through tension and not compression (*positive cable tension*). This limitation creates challenging problems in the control of the manipulator [15] and workspace

determination. It also means that techniques to determine the workspace for serial and rigid link parallel manipulators are not directly applicable to cable manipulators due to this unilateral property. Several types of cable driven parallel manipulator workspace have been identified and investigated, such as the *static workspace* [16], *dynamic workspace* [17], *wrench-feasible workspace* [18] [19] [20], *wrench-closure workspace* [20] [21] [22] [23] [24], and *interference-free workspace* [25] [26]. The *wrench-feasible workspace* (WFW) for the manipulator refers to the set of poses for which the system dynamics can be satisfied with positive cable tensions for a specified set of external wrenches, velocities, and accelerations, within the specified actuation limits of the cable. *The wrench-closure workspace* (WCW) is similar to the WFW, defined as the set of poses in which the manipulator can sustain any arbitrary external wrench when no upper bounds are placed on the cable tensions.

Cable manipulators with n degrees-of-freedom (DOF) actuated by m cables can be classified as being incompletely restrained $(m < n+1)$, completely restrained $(m = n+1)$, or redundantly restrained $(m > n+1)$ [27]. Techniques to determine the WCW for redundantly restrained systems have been studied in [21] [23] based on the concept of determining the positive spanning of the task space and on convex analysis, while completely restrained systems were studied in [22]. For redundantly restrained manipulators, workspace can be determined by considering the system as a combinatorial set of completely restrained systems. Approaches for workspace determination can be classified as numerical [21] [22] or analytical [17] [19] [23] [24].

Numerical methods are typically point-wise evaluation techniques, where the task space is exhaustively searched at discrete intervals. This approach provides only a local measure of the workspace at the evaluated points, suffering from the effects of discretisation. The accuracy for this approach is dependent on the interval width (*step-size*), where decreased width results in increased accuracy. The drawback of decreasing interval width is that the computational time will be significantly increased.

Analytical formulations provide a more accurate description of workspace and insights into its geometry. The region can be described as the intersection of a set of inequality equations. Due to the algebraic complexity, previous studies have been concerned with determining only the boundary of the workspace. In [23], the WCW boundary for over-restrained planar cable robots in constant orientation was analytically studied. The boundary was determined to be in the form of a set of second degree conic sections of two variables. In a similar manner, it was shown in [24] that the form for WCW of planar cable manipulators could be expressed as a polynomial of degree 12 in three variables. A similar problem was investigated in [19], where the WFW boundary for a range of systems, planar, spatial and point mass cable robots in constant orientation were analytically determined. The solution was shown to be comprised of a set of lower and upper boundaries. For the spatial manipulator, the lower boundary is a set of fifth degree polynomial equations in three variables with 56 polynomial coefficients. The upper boundary was observed to be generally not polynomial and hence difficult to solve. Upon determining the boundaries, the workspace itself can then be located by graphically identifying the regions that satisfy the set of inequalities. The manipulator designer can take advantage of this insight into the workspace geometry while graphically identifying the workspace region. Many existing analytical methods where only boundaries of the workspace are determined require additional steps to determine the admitted workspace. Compared to the techniques under numerical approach, the analytical approach typically provides only qualitative information regarding the workspace. The ability to quantitatively describe the generated region is important in determining the cable mounting locations given the desired workspace characteristics. This also allows an automated design process of a mechanism, where quality functions associated with various desired features in the design can be incorporated.

In this paper, an approach to generate the WCW using a hybrid of analytical and numerical methods for completely restrained cable driven manipulators is presented. The analytical solution for the WCW is reduced to a set of univariate polynomial inequalities with respect to a single pose variable by treating the other remaining pose variables as constants. The constant pose variables are then discretely varied over the range of interest, and the analytical form is accurately solved at each iteration. The workspace region can then be determined directly by solving the set of univariate polynomial inequalities. Compared to the conventional point-wise evaluation methods, the proposed technique has the advantages of lower computational complexity and increased accuracy. It is shown that the reduction of the computational speed achieved by the proposed algorithm against the traditional point-wise approach increases with finer evaluation step-size and higher system complexity.

For the test cases presented in this paper, a computational time saving of at least 4 folds for coarse step-sizes and up to orders of magnitude of saving for finer resolutions is achieved. The improvement in computational speed does not guarantee real-time evaluation of a manipulator workspace, as it is dependent of evaluation step-size and system complexity. However, the multiple folds of saving in computational time translates into tremendous advantage in iterative processes, such as in the design of cable manipulators to achieve optimal workspace [12] [14], resulting in a significant savings in design costs. Another benefit of the proposed approach is the ease and efficiency in which the quality of the workspace in the form of cost functions can be included and evaluated quantitatively.

The remainder of this paper is organised as follows: Section 2 describes the kinematics and dynamics model for a general spatial cable-driven manipulator. The wrench-closure condition and the corresponding wrench-closure workspace is presented in Section 3. Section 4 describes the proposed workspace determination approach for a general 6-DOF spatial

manipulator and a 3-DOF ball joint manipulator. The potential of incorporating quality functions to quantitatively evaluate the resulting WCW is also discussed. The simulation setup for the 3-DOF and 6-DOF manipulators will be presented in Section 5. Section 6 presents and compares the resulting workspace from the proposed and numerical approaches. Finally, Section 7 concludes the paper and presents areas of future work.

2 Kinematic and Dynamic Model

The model for a general 6-DOF spatial cable driven parallel manipulator is shown in Figure 1. The cables are attached to the base frame at positions $\mathbf{r}_A$, and to the end effector at positions $\mathbf{r}_B$. Vectors $\mathbf{r}_A$ and $\mathbf{r}_B$ are constant in the inertial frame, $\{F_0\}$, and end effector frame, $\{F_E\}$, respectively. The attachment points for cable i can be represented as:

$$\begin{aligned} {}^0\mathbf{r}_{A_i} &= r_{A_{ix}}\mathbf{i}_0 + r_{A_{iy}}\mathbf{j}_0 + r_{A_{iz}}\mathbf{k}_0 \\ {}^E\mathbf{r}_{B_i} &= r_{B_{ix}}\mathbf{i}_e + r_{B_{iy}}\mathbf{j}_e + r_{B_{iz}}\mathbf{k}_e \end{aligned} \tag{1}$$

where ${}^0\mathbf{r}$ and ${}^E\mathbf{r}$ represents the vector $\mathbf{r}$ in $\{F_0\}$ and $\{F_E\}$, respectively.

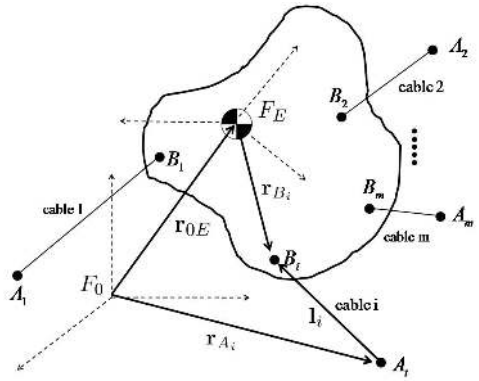

Fig. 1. General Model for Cable Manipulator

The cable vector can be kinematically defined as:

$$\mathbf{l}_i = \mathbf{r}_{0E} + \mathbf{r}_{B_i} - \mathbf{r}_{A_i} \tag{2}$$

Expressing the dynamics of the system in Lagrangian form, the equations of motion for the 6-DOF m-cable system can be defined as:

$$M(\mathbf{x})\ddot{\mathbf{x}} + C(\mathbf{x},\dot{\mathbf{x}}) + G(\mathbf{x}) + F_{ext}(\mathbf{x}) = -J^T(\mathbf{x})\mathbf{t} \tag{3}$$

where $\mathbf{x}$ is the manipulator pose, $M(\mathbf{x})$, $C(\mathbf{x},\dot{\mathbf{x}})$, $G(\mathbf{x})$, and $F_{ext}(\mathbf{x})$ are the mass inertia matrix, centrifugal and Coriolis force vector, gravitational vector, and external wrench vector, respectively. The cable wrench vector is denoted by $-J^T\mathbf{t}$, where $-J^T(\mathbf{x})$ represents the direction of the forces and moments generated by the actuated cables, and $\mathbf{t} = \begin{bmatrix} t_1 & t_2 & \dots & t_m \end{bmatrix}^T$ is the cable force vector containing the magnitudes of the tension for individual cables, where t_i is the tension in cable i. The positive tension constraint is denoted by $\mathbf{t} > \mathbf{0}$, that is, all the cable tension magnitudes, t_i, are required to be positive. The $6 \times m$ transpose of the Jacobian matrix is defined as:

$$J^T = \begin{bmatrix} \hat{\mathbf{l}}_1 & \hat{\mathbf{l}}_2 & \dots & \hat{\mathbf{l}}_m \\ \mathbf{r}_{B_1} \times \hat{\mathbf{l}}_1 & \mathbf{r}_{B_2} \times \hat{\mathbf{l}}_2 & \dots & \mathbf{r}_{B_m} \times \hat{\mathbf{l}}_m \end{bmatrix} \tag{4}$$

Expressing J^T terms in the inertial frame in terms of the cable attachment points and manipulator pose:

$$
\begin{aligned}
{}^0\hat{\mathbf{l}}_i &= \frac{\mathbf{r}_{0E}(\mathbf{x}) + {}^0_E R(\mathbf{x})\mathbf{r}_{B_i} - \mathbf{r}_{A_i}}{l_i} \\
{}^0\mathbf{r}_{B_i} \times {}^0\hat{\mathbf{l}}_i &= \frac{({}^0_E R(\mathbf{x})\mathbf{r}_{B_i}) \times (\mathbf{r}_{0E}(\mathbf{x}) - \mathbf{r}_{A_i})}{l_i}
\end{aligned} \tag{5}
$$

where l_i is the length of the cable i, and ${}^0_E R$ is the rotation matrix from the frame $\{F_0\}$ to $\{F_E\}$, which is dependent on the manipulator pose.

3 Wrench-Closure Workspace

The *wrench-closure condition* (WCC) for a particular pose is satisfied if a set of positive cable tensions can be determined for any arbitrary external wrench, velocity or acceleration of the manipulator without any upper bound to cable tension. Combining the terms representing the dynamics of the system, the equation of motion (3) can be expressed as:

$$
\mathbf{w} = J^T \mathbf{t} \tag{6}
$$

where $\mathbf{w} = -[M(\mathbf{x})\ddot{\mathbf{x}} + C(\mathbf{x}, \dot{\mathbf{x}}) + G(\mathbf{x}) + F_{ext}(\mathbf{x})]$. Hence for an n-DOF m-cable system, the WCC can be described as:

$$
\forall \mathbf{w} \in \mathbb{R}^n, \exists \mathbf{t} > \mathbf{0} : J^T \mathbf{t} = \mathbf{w} \tag{7}
$$

The geometrical interpretation of (7) is that the WCC is satisfied if the columns of J^T positively span $\mathbb{R}^n$ for full rank J^T. An equivalent definition of the WCC is the existence of some positive cable tension vector within the nullspace of J^T [23].

$$
\begin{aligned}
&rank(J^T) = n \\
&\exists \mathbf{t} \in ker(J^T) : \mathbf{t} > 0
\end{aligned} \tag{8}
$$

Another interpretation of (7) is that the WCC can be described by performing row reduction on the linear system. Since J^T is of full rank, and considering a completely restrained system, $m = n+1$, the $n \times (n+1)$ transpose of the Jacobian matrix can be expressed in reduced row echelon form:

$$
J^T \rightarrow \left[I_n \middle| \mathbf{v}(\mathbf{x}) \right] \tag{9}
$$

where $I_n \in \mathbb{R}^{n \times n}$ is an identity matrix and $\mathbf{v} \in \mathbb{R}^n$ is a function of the pose variables. Applying the row reduction as in (9) on the WCC in (7):

$$
\left[I_n \middle| \mathbf{v}(\mathbf{x}) \right] \mathbf{t} = \mathbf{w}', \mathbf{t} > \mathbf{0} \tag{10}
$$

where $\mathbf{w}'$ is the wrench vector after row reduction. The interpretation of (10) is that if all components of $\mathbf{v}$ are negative, $\mathbf{v} < \mathbf{0}$, then the WCC is satisfied. This can be shown by observing the set of equations from (10):

$$
t_j + v_j(\mathbf{x}) t_m = w'_j, \forall j \in 1, \ldots, n \tag{11}
$$

where j refers to the j^{th} row of (10). Given that $t_m \in (0, \infty)$, if $v_j(\mathbf{x}) < 0$, then $v_j t_m \in (-\infty, 0)$ and hence $w'_j \in (-\infty, \infty)$. The result of this is $\mathbf{w} \in \mathbb{R}^n$, satisfying the WCC from (7). The WCW for the manipulator is defined as the set of poses in which the WCC is satisfied. This can be defined as:

$$
\{\mathbf{x} : \forall \mathbf{w} \in \mathbb{R}^n, \exists \mathbf{t} > \mathbf{0}, J^T(\mathbf{x})\mathbf{t} = \mathbf{w}\} \tag{12}
$$

An alternative definition of WCC in (10) can also be used to define the WCW:

$$\left\{\mathbf{x} : \mathbf{v}(\mathbf{x}) < \mathbf{0}, J^T \rightarrow \left[I_n \middle| \mathbf{v}(\mathbf{x}) \right] \right\} \tag{13}$$

Hence the resulting workspace can be considered as the intersection of a set of multivariate inequalities. Knowledge of the algebraic form of $\mathbf{v}(\mathbf{x})$, derived in the following section, is required to analytically determine the workspace region. It can also be shown that the WCW boundary is comprised of sections of the curves $\mathbf{v}(\mathbf{x}) = \mathbf{0}$.

4 Proposed Workspace Determination Approach

4.1 6-DOF Spatial Manipulator

The analytical form for the WCW of a general 6-DOF spatial manipulator based on (13) is presented in this section. The pose for the manipulator as shown in Figure 1 can be defined as $\mathbf{x} = [x\ y\ z\ \alpha\ \beta\ \gamma]^T$, where x, y and z are the translation variables between the origin of the inertial and end-effector coordinate frames, and α, β and γ are the *xyz*-Euler angles that define the orientation of the manipulator. The relationship between $\{F_0\}$ and $\{F_E\}$ can be described as:

$$\begin{aligned} \mathbf{r}_{0E} &= x\mathbf{i}_0 + y\mathbf{j}_0 + z\mathbf{k}_0 \\ {}^0_E R &= \begin{bmatrix} c_\beta c_\gamma & -c_\beta s_\gamma & s_\beta \\ c_\alpha s_\gamma + s_\alpha s_\beta c_\gamma & c_\alpha c_\gamma - s_\alpha s_\beta s_\gamma & -s_\alpha c_\beta \\ s_\alpha s_\gamma - c_\alpha s_\beta c_\gamma & s_\alpha c_\gamma + c_\alpha s_\beta s_\gamma & c_\alpha c_\beta \end{bmatrix} \end{aligned} \tag{14}$$

where c_α, c_β and c_γ, and s_α, s_β and s_γ represent $\cos\alpha, \cos\beta$ and $\cos\gamma$, and $\sin\alpha, \sin\beta$ and $\sin\gamma$, respectively. Without loss of generality, the cable attachment locations from (1) can be used. The i^{th} column of J^T matrix (4) can be expressed as:

$$\begin{bmatrix} \hat{\mathbf{l}}_i \\ \mathbf{r}_{EB_i} \times \hat{\mathbf{l}}_i \end{bmatrix} = \frac{1}{l_i} \begin{bmatrix} J_{1i} \\ J_{2i} \\ J_{3i} \\ J_{4i} \\ J_{5i} \\ J_{6i} \end{bmatrix} \tag{15}$$

where each of the terms can be explicitly derived as:

$$\begin{aligned} J_{1i} &= x + r_{B_{ix}} c_\beta c_\gamma - r_{B_{iy}} c_\beta s_\gamma + r_{B_{iz}} s_\beta - r_{A_{ix}} \\ J_{2i} &= y + r_{B_{ix}}(c_\alpha s_\gamma + s_\alpha s_\beta c_\gamma) + r_{B_{iy}}(c_\alpha c_\gamma - s_\alpha s_\beta s_\gamma) - r_{B_{iz}} s_\alpha c_\beta - r_{A_{iy}} \\ J_{3i} &= z + r_{B_{ix}}(s_\alpha s_\gamma - c_\alpha s_\beta c_\gamma) + r_{B_{iy}}(s_\alpha c_\gamma + c_\alpha s_\beta s_\gamma) + r_{B_{iz}} c_\alpha c_\beta - r_{A_{iz}} \\ J_{4i} &= (r_{B_{ix}}(c_\alpha s_\gamma + s_\alpha s_\beta c_\gamma) + r_{B_{iy}}(c_\alpha c_\gamma - s_\alpha s_\beta s_\gamma) - r_{B_{iz}} s_\alpha c_\beta)(z - r_{A_{iz}}) \\ &\quad -(r_{B_{ix}}(s_\alpha s_\gamma - c_\alpha s_\beta c_\gamma) + r_{B_{iy}}(s_\alpha c_\gamma + c_\alpha s_\beta s_\gamma) + r_{B_{iz}} c_\alpha c_\beta)(y - r_{A_{iy}}) \\ J_{5i} &= -(r_{B_{ix}} c_\beta c_\gamma - r_{B_{iy}} c_\beta s_\gamma + r_{B_{iz}} s_\beta)(z - r_{A_{iz}}) \\ &\quad +(r_{B_{ix}}(s_\alpha s_\gamma - c_\alpha s_\beta c_\gamma) + r_{B_{iy}}(s_\alpha c_\gamma + c_\alpha s_\beta s_\gamma) + r_{B_{iz}} c_\alpha c_\beta)(x - r_{A_{ix}}) \\ J_{6i} &= (r_{B_{ix}} c_\beta c_\gamma - r_{B_{iy}} c_\beta s_\gamma + r_{B_{iz}} s_\beta)(y - r_{A_{iy}}) \\ &\quad -(r_{B_{ix}}(c_\alpha s_\gamma + s_\alpha s_\beta c_\gamma) + r_{B_{iy}}(c_\alpha c_\gamma - s_\alpha s_\beta s_\gamma) - r_{B_{iz}} s_\alpha c_\beta)(x - r_{A_{ix}}) \end{aligned} \tag{16}$$

Previous analytical studies typically assume constant orientation, by treating pose variables, α, β and γ, as constants [20] [21] [22]. This reduces the complexity of the workspace boundary to a set of multivariate polynomial equations. In comparison, the solution for the WCW from (13) is a set of multivariate inequalities that are generally not polynomials. The analytical solution can be simplified by expressing the WCW as a function of a single variable, and treating the remaining variables as constant values. As a result, the WCW can be reduced to a set of univariate polynomial inequalities. Any of the six pose variables for the spatial manipulator could be selected to be solved analytically, resulting in different polynomial complexities.

Consider an example where the WCW was to be expressed with respect to the translational pose variable x. It can be observed that the term J_{1i} from (16) is a linear function of x expressed in the form:

$$\begin{aligned} J_{1i} &= ax + b \in O(x) \\ a &= 1 \\ b &= r_{B_{ix}} c_\beta c_\gamma - r_{B_{iy}} c_\beta s_\gamma + r_{B_{iz}} s_\beta - r_{A_{ix}} \end{aligned} \quad (17)$$

Repeating this analysis on the remaining terms of J^T result in the following algebraic complexities:

$$\begin{aligned} J_{1i}, J_{5i}, J_{6i} &\in O(x) \\ J_{2i}, J_{3i}, J_{4i} &\in O(1) \end{aligned} \quad (18)$$

where the coefficients of the terms are a function of the constant pose variables y, z, α, β, and γ. The order of complexity for the terms of J^T can be expressed as:

$$J^T \in \begin{bmatrix} \frac{O(x)}{l_1} & \frac{O(x)}{l_2} & \frac{O(x)}{l_3} & \frac{O(x)}{l_4} & \frac{O(x)}{l_5} & \frac{O(x)}{l_6} & \frac{O(x)}{l_7} \\ \frac{O(1)}{l_1} & \frac{O(1)}{l_2} & \frac{O(1)}{l_3} & \frac{O(1)}{l_4} & \frac{O(1)}{l_5} & \frac{O(1)}{l_6} & \frac{O(1)}{l_7} \\ \frac{O(1)}{l_1} & \frac{O(1)}{l_2} & \frac{O(1)}{l_3} & \frac{O(1)}{l_4} & \frac{O(1)}{l_5} & \frac{O(1)}{l_6} & \frac{O(1)}{l_7} \\ \frac{O(1)}{l_1} & \frac{O(1)}{l_2} & \frac{O(1)}{l_3} & \frac{O(1)}{l_4} & \frac{O(1)}{l_5} & \frac{O(1)}{l_6} & \frac{O(1)}{l_7} \\ \frac{O(x)}{l_1} & \frac{O(x)}{l_2} & \frac{O(x)}{l_3} & \frac{O(x)}{l_4} & \frac{O(x)}{l_5} & \frac{O(x)}{l_6} & \frac{O(x)}{l_7} \\ \frac{O(x)}{l_1} & \frac{O(x)}{l_2} & \frac{O(x)}{l_3} & \frac{O(x)}{l_4} & \frac{O(x)}{l_5} & \frac{O(x)}{l_6} & \frac{O(x)}{l_7} \end{bmatrix} \quad (19)$$

The complexity of the terms in the vector $\mathbf{v}$ from (9) can be determined by applying row reduction on J^T from (19). It can be shown that after row reduction, $v_j(x)$ can be expressed in the form of $\frac{l_j}{l_7} \frac{p_j(x)}{d(x)}$, where l_j is the length of cable j, and $p_j, d \in O(x^3)$ are univariate cubic equations. The WCW from (13) can be expressed as:

$$\left\{ x : v_j(x) = \frac{l_j}{l_7} \frac{p_j(x)}{d(x)} < 0, \forall v_j(x) \in \mathbf{v}(x) \right\} \quad (20)$$

Since cable lengths are strictly positive, $l_j > 0$, these non-polynomial terms can be ignored. Considering the numerator and denominator polynomial equations separately, the WCW definition from (20) can be expressed as a univariate equation:

$$\{x : sgn(p_j(x)) = -sgn(d(x)), p_j(x) \neq 0 \;\; \forall j \in \{1, \ldots, 6\}, d(x) \neq 0\} \quad (21)$$

The resulting workspace can be represented as a set of open intervals, $x \in (x_l, x_u)$, where x_l and x_u form the workspace boundaries. Given that p_j and d are cubic equations, its roots and sgn regions can be expressed explicitly in analytical form. Alternatively, (21) can be expressed as a set of univariate polynomial inequalities. Algorithm 1 summarises this approach for a general case n-DOF system.

Algorithm 1 Determining the values of x for which $\mathbf{v}(x) < \mathbf{0}$

Require: $\mathbf{v}(x) \in \mathbb{R}^n$
Ensure: $\mathbf{v}(x) < \mathbf{0}$
  $d(x) \Leftarrow$ univariate polynomial equation from $\mathbf{v}(x)$ (Eqn. 20)
  for $i = 1$ to n **do**
    $p_i(x) \Leftarrow$ univariate polynomial equation from $\mathbf{v}(x)$ (Eqn. 20)
    $W_i = \{x : p_i(x) < 0, d(x) > 0\} \cup \{x : p_i(x) > 0, d(x) < 0\}$ (Eqn. 21)
  end for
  return $W_1 \cap W_2 \cap \cdots \cap W_n$

Repeating this analysis, if the WCW was to be expressed as a function of an orientation pose variable, for example, β, then the complexity of the Jacobian terms from (16) are:

$$J_{1i}, J_{2i}, J_{3i}, J_{4i}, J_{5i}, J_{6i} \in O(c_\beta + s_\beta) \tag{22}$$

Using the Jacobian terms from (22), expressing $v_j(\beta)$ as $\frac{l_j}{l_7}\frac{p_j(\beta)}{d(\beta)}$ yields $p_j, d \in O(c_\beta^6 + s_\beta^6)$. The transcendental terms can be eliminated by introducing the Weierstrass substitution:

$$T = \tan\frac{\beta}{2},\ \sin\beta = \frac{2T}{1+T^2},\ \cos\beta = \frac{1-T^2}{1+T^2} \tag{23}$$

As a result, $p_j(T), d(T) \in O(T^{12})$ become univariate polynomials of degree 12, where the set of constant pose variables are contained within the polynomial coefficients.

Performing this analysis for each of the pose variables, it can be shown that the polynomial complexities for p_j and d will differ. Selection of translational variables x, y or z results in univariate cubic equations, $p_j(T), d(T) \in O(T^3)$, while selecting the orientation variable α yields degree 10 univariate polynomials, $p_j(T), d(T) \in O(T^{10})$ and orientation variable β or γ degree 12 univariate polynomials, $p_j(T), d(T) \in O(T^{12})$. From this analysis, it is apparent that different complexities of polynomial equations arise depending on the degrees of freedom and pose representation for the manipulator. For workspace determination, the pose variable that results in the simplest form should be chosen. The summary of the algorithm when implemented to determine WCW for an n-DOF completely restrained cable system is given in Algorithm 2.

Algorithm 2 Determining WCW for an n-DOF $(n+1)$-cable system

Require: $\{B_1, B_2, \ldots, B_n\}$ which are the bounds for variables $\{x_1, x_2, \ldots, x_n\}$
Ensure: W is the WCW workspace of manipulator
  $\mathbf{x} \Leftarrow \{x_1, x_2, \ldots, x_n\} \in \mathbb{R}^n$ (pose variable vector)
  $J^T \Leftarrow n \times (n+1)$ transpose of Jacobian matrix (Eqn. 4)
  for all $J_{ij} \in J^T$ **do**
    $J_{ij} \Leftarrow$ derive analytical expression (Eqn. 16)
  end for
  $\mathbf{v}(\mathbf{x}) \Leftarrow (n+1)^{\text{th}}$ column of row-reduced J^T matrix (Eqn. 9)
  $x_s \Leftarrow$ selected pose variable from $\mathbf{x}$, e.g. x_n
  $\mathbf{x}_c \Leftarrow \{x_1, x_2, \ldots, x_{n-1}\} \in \mathbb{R}^{n-1}$ where $x_s \notin \mathbf{x}_c$; $\mathbf{x}_c$ contains the remaining pose variables
  for $x_1 \in B_1$ with step-size ΔB_1 **do**
    for $x_2 \in B_2$ with step-size ΔB_2 **do**
      $\vdots$
      for $x_{n-1} \in B_{n-1}$ with step-size ΔB_{n-1} **do**
        $\mathbf{v}(x_s) \Leftarrow$ substitute $\mathbf{x}_c$ into $\mathbf{v}(\mathbf{x})$ (Eqn. 20)
        $A \Leftarrow$ region satisfying $\mathbf{v}(x_s) < \mathbf{0}$ (Algorithm 1)
        $W \Leftarrow W \cup A$
      end for
      $\vdots$
    end for
  end for
  return W

4.2 3-DOF Ball Joint Manipulator

A 3-DOF manipulator constrained at the origin of the inertial frame, $\{F_0\}$, by a ball joint is shown in Figure 2. The pose of the manipulator can be defined by the xyz-Euler orientation angles $\mathbf{x} = [\alpha\ \beta\ \gamma]^T$. Since there are only orientation degrees of freedom, the transpose of the Jacobian matrix is:

$$J^T = \left[\, \mathbf{r}_{B_1} \times \hat{\mathbf{l}}_1\ \mathbf{r}_{B_2} \times \hat{\mathbf{l}}_2\ \mathbf{r}_{B_3} \times \hat{\mathbf{l}}_3\ \mathbf{r}_{B_4} \times \hat{\mathbf{l}}_4 \,\right] \tag{24}$$

The Jacobian matrix terms in (24) are equivalent to (5) where $\mathbf{r}_{0E} = \mathbf{0}$:

$$\mathbf{r}_{B_i} \times \hat{\mathbf{l}}_i = \frac{\mathbf{r}_{A_i} \times ({}^0_E R(\mathbf{x})\mathbf{r}_{B_i})}{l_i} \tag{25}$$

From (15), it can seen that the Jacobian terms for the particular system can be expressed as:

$$\left[\, \mathbf{r}_{EB_i} \times \hat{\mathbf{l}}_i \,\right] = \frac{1}{l_i} \begin{bmatrix} J_{1i} \\ J_{2i} \\ J_{3i} \end{bmatrix} \tag{26}$$

where each term could be explicitly derived from (25):

$$\begin{aligned}
J_{1i} &= r_{A_{iy}}(r_{B_{ix}}(s_\alpha s_\gamma - c_\alpha s_\beta c_\gamma) + r_{B_{iy}}(s_\alpha c_\gamma + c_\alpha s_\beta s_\gamma) + r_{B_{iz}} c_\alpha c_\beta) \\
&\quad - r_{A_{iz}}(r_{B_{ix}}(c_\alpha s_\gamma + s_\alpha s_\beta c_\gamma) + r_{B_{iy}}(c_\alpha c_\gamma - s_\alpha s_\beta s_\gamma) - r_{B_{iz}} s_\alpha c_\beta) \\
J_{2i} &= -r_{A_{ix}}(r_{B_{ix}}(s_\alpha s_\gamma - c_\alpha s_\beta c_\gamma) + r_{B_{iy}}(s_\alpha c_\gamma + c_\alpha s_\beta s_\gamma) + r_{B_{iz}} c_\alpha c_\beta) \\
&\quad + r_{A_{iz}}(r_{B_{ix}} c_\beta c_\gamma - r_{B_{iy}} c_\beta s_\gamma + r_{B_{iz}} s_\beta) \\
J_{3i} &= r_{A_{ix}}(r_{B_{ix}}(c_\alpha s_\gamma + s_\alpha s_\beta c_\gamma) + r_{B_{iy}}(c_\alpha c_\gamma - s_\alpha s_\beta s_\gamma) - r_{B_{iz}} s_\alpha c_\beta) \\
&\quad - r_{A_{iy}}(r_{B_{ix}} c_\beta c_\gamma - r_{B_{iy}} c_\beta s_\gamma + r_{B_{iz}} s_\beta)
\end{aligned} \tag{27}$$

The problem can then be reformulated as a univariate polynomial function of one of the pose variables. In this case, the three possible Euler angles will yield the same level of complexity. To illustrate this example, α was selected, and the complexity of the Jacobian terms are:

$$J_{1i}, J_{2i}, J_{3i} \in O(c_\alpha + s_\alpha) \tag{28}$$

where the coefficients of the terms are a function of β and γ. After row-reduction on J^T, $v_j(\alpha) = \frac{l_j}{l_4}\frac{p_j(\alpha)}{d(\alpha)}$, where $p_j, d \in O(c_\alpha^3 + s_\alpha^3)$. Introducing the Weierstrass substitution in (23), univariate sextics, $p_j, d \in O(T^6)$, are obtained. Hence the WCW definition for this specific manipulator becomes:

$$W = \{\alpha : T = \tan\frac{\alpha}{2}, sgn(p_j(T)) = -sgn(d(T)), p_j(T) \neq 0 \;\; \forall j \in \{1,\ldots,3\}, d(x) \neq 0\} \tag{29}$$

The resulting workspace can be represented as a set of open intervals, $\alpha \in (\alpha_l, \alpha_u)$, where α_l and α_u form the workspace boundaries.

4.3 Workspace Evaluation

The proposed technique inherently accommodates the ability to quantitatively evaluate the WCW in an efficient manner. This is crucial in the optimisation of cable configurations for a particular manipulator design. In the optimisation process, the evaluation of workspace under a desired quantitative measure of quality is required. A trivial example of such a function is the total workspace volume. More sophisticated functions could incorporate levels of desirability in different workspace regions.

Considering the quality of the workspace at a particular pose, $\mathbf{x}$, as $f(\mathbf{x})$, the total quality of the workspace can be defined as:

$$Q = \int_W f(\mathbf{x}) d\mathbf{x} \tag{30}$$

where W represents the WCW of the manipulator. It will be shown that the total workspace quality could be efficiently computed if the integral function of $f(\mathbf{x})$ can be determined analytically with respect to at least one of the pose variables.

For example, considering the 3-DOF ball joint manipulator presented in Section 4.2, the total quality from (30) can be expressed as:

$$Q = \int_{\alpha}\int_{\beta}\int_{\gamma} f(\alpha,\beta,\gamma)\, d\alpha\, d\beta\, d\gamma,\ \forall(\alpha,\beta,\gamma) \in W \tag{31}$$

Assuming that the integral of $f(\alpha,\beta,\gamma)$ can be determined with respect to α, $F(\alpha)$, the quality from (31) can be expressed as:

$$\begin{aligned} Q &= \sum_{\gamma}\sum_{\beta}\sum_{k}\int_{\alpha_{u_l}}^{\alpha_{u_k}} f(\alpha,\beta,\gamma)d\alpha,\ \forall(\beta,\gamma) \in W \\ &= \sum_{\gamma}\sum_{\beta}\sum_{k} F(\alpha_{u_k}) - F(\alpha_{u_l}),\ \forall(\beta,\gamma) \in W \end{aligned} \tag{32}$$

where k represents the number of (α_l, α_u) intervals at particular β and γ values. The total quality from (32) provides an efficient way to evaluate the workspace by using the lower and upper bounds determined by the analytical WCW form from (29). In comparison, the workspace determined by the point-wise approach would require evaluation of $f(\alpha,\beta,\gamma)$ at each (α,β,γ) pose within the WCW. A simple and intuitive quality function is the volume of the workspace, where $f(\alpha,\beta,\gamma) = 1$ and hence $F(\alpha) = \alpha$. The resulting total cost can be expressed as:

$$Q = \sum_{\gamma}\sum_{\beta}\sum_{k}(\alpha_{u_k} - \alpha_{u_l}),\ \forall(\beta,\gamma) \in W \tag{33}$$

With careful selection of the quality functions, the manipulator's cable configuration can be optimised to possess desirable WCW characteristics in an efficient and autonomous manner.

5 Simulation Setup

The WCW for a 3-DOF and 6-DOF completely restrained cable driven parallel manipulator is generated using the proposed hybrid approach. The workspace for the 3-DOF manipulator will also be determined using the point-wise approach as a benchmark in terms of accuracy and computational efficiency. The point-wise approach to determine the WCW for a 6-DOF manipulator was not performed due to the inefficiency of the method. The simulation setup and manipulator cable arrangements are presented in this section.

5.1 3-DOF Ball Joint Manipulator

The cable attachment points for the proposed 3-DOF manipulator as shown in Figure 2 are displayed in Table 1, assuming units in metres. In this configuration, the cables are located symmetrically around the ball joint of the manipulator.

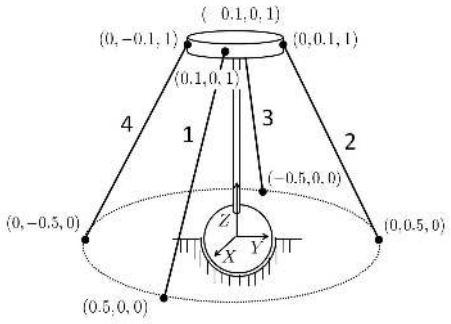

Fig. 2. 3-DOF Ball Joint Manipulator Model

For this manipulator, the bounds for the pose variables in determining the workspace were selected to be $\alpha,\beta \in \left[-\frac{\pi}{2}, \frac{\pi}{2}\right]$ rad and $\gamma \in [-\pi, \pi]$ rad. A range of step sizes, $\Delta\alpha$, $\Delta\beta$ and $\Delta\gamma$, were varied to observe the efficiency and accuracy of both

Table 1. Cable Configuration for 3-DOF Manipulator

	Base			End Effector		
	${}^0r_{A_{ix}}$	${}^0r_{A_{iy}}$	${}^0r_{A_{iz}}$	${}^Er_{B_{ix}}$	${}^Er_{B_{iy}}$	${}^Er_{B_{iz}}$
Cable 1	0.5	0	0	0.1	0	1
Cable 2	0	0.5	0	0	0.1	1
Cable 3	−0.5	0	0	−0.1	0	1
Cable 4	0	−0.5	0	0	−0.1	1

techniques. The efficiency of the approach was measured as the computational time required to determine the workspace, and accuracy was compared through graphical representations of the WCW and workspace volumes.

Due to discretisation in the approaches, the workspace volume for the point-wise approach can be considered as a sum of elementary cubes with volume $\Delta V = \Delta\alpha \cdot \Delta\beta \cdot \Delta\gamma$, and the whole volume of the workspace can be expressed as:

$$V_a = \sum_{\alpha}\sum_{\beta}\sum_{\gamma} \Delta\alpha \cdot \Delta\beta \cdot \Delta\gamma \tag{34}$$

For the proposed hybrid approach, the workspace volume can be considered as a sum of thin rectangles with volume $\Delta V = \Delta\beta \cdot \Delta\gamma \cdot (\alpha_u - \alpha_l)$, hence the total volume can be represented as:

$$V_b = \sum_{\beta}\sum_{\gamma}\sum_{k} \Delta\beta \cdot \Delta\gamma \cdot (\alpha_{u_k} - \alpha_{l_k}) \tag{35}$$

where k represents the number of (α_l, α_u) intervals at the β and γ value. Since the point-wise approach is known to underestimate the workspace, the difference in volumes of the two approaches can be expressed by taking a ratio of the volumes from (34) and (35). If the same step size values, $\Delta\beta$ and $\Delta\gamma$, are used in both approaches, the volume ratio can be expressed as:

$$V_r = \frac{V_a}{V_b} = \frac{\sum_{\beta}\sum_{\gamma}\sum_{\alpha} \Delta\alpha}{\sum_{\beta}\sum_{\gamma}\sum_{k} (\alpha_{u_k} - \alpha_{l_k})} \tag{36}$$

To allow direct comparison of the point-wise approach against the proposed approach, it is assumed that continuous points along α can be considered as a single linear region, relaxing the locality constraint of the point-wise method.

5.1.1 Proposed Hybrid Analytical-Numerical Approach

It was shown in Section 4.2 that the polynomial coefficients for the WCW in (29) will be functions of β and γ. By assuming constant β and γ, polynomial coefficients and subsequently, the solution to the WCW with respect to α, can be determined. In this simulation, β and γ are uniformly varied within the defined bounds as shown in Algorithm 2. At each β and γ iteration, the Weierstrass substitution is applied and the roots of the polynomial equations, $p_1(T), p_2(T), p_3(T)$ and $d(T)$ are determined. This is used to evaluate the sign of the polynomial functions and then to generate the WCW using (29). The proposed approach provides a point-based measure along β and γ, while the WCC is satisfied continuously along $\alpha_l < \alpha < \alpha_u$. The only inaccuracy incurred in this approach is the numerical error involved in solving for the polynomial roots. To determine the computational complexity of the proposed approach, the number of steps for the pose variables α, β and γ can be denoted as a, b and c, respectively. Since only β and γ are varied iteratively, the complexity is $O(bc)$, with the fundamental operation of solving for (29) at each iteration.

5.1.2 Point-Wise Evaluation

In the point-wise evaluation approach, pose variables are varied discretely within the defined bounds. At each sample point, if the WCC from (13) is satisfied, then the point can be classified as being within the WCW. Workspace obtained through this approach has two main features: identified regions are a collection of points that satisfy WCC locally, and the

obtained region underestimate the exact workspace. The first feature implies that the resulting workspace region will be described by a set of points, where the workspace properties between points cannot be concluded. Underestimation of the workspace means that the determined region only approximates the exact solution. As a result, the accuracy is dependent on the step-sizes, $\Delta\alpha$, $\Delta\beta$ and $\Delta\gamma$. In this simulation experiment, the pose variables α, β and γ are varied at uniform intervals, implying that $\Delta\alpha$, $\Delta\beta$ and $\Delta\gamma$ are constant values. Hence, the computational complexity of the uniform interval point-wise approach is $O(abc)$, with the fundamental operation as the verification of the WCC from (13).

5.2 6-DOF Spatial Manipulator

The general 6-DOF spatial manipulator analysed is of the same type as investigated in [18] [21], consisting of a floating end effector with cables attached to a base frame, as shown in Figure 3. The cable attachment points for the manipulator are displayed in Table 2.

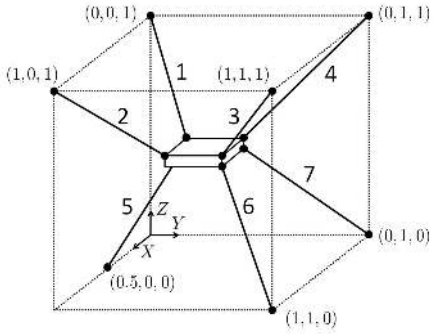

Fig. 3. 6-DOF Ball Joint Manipulator Model

Table 2. Cable Configuration for 6-DOF Manipulator

	Base			End Effector		
	${}^0r_{A_{ix}}$	${}^0r_{A_{iy}}$	${}^0r_{A_{iz}}$	${}^Er_{B_{ix}}$	${}^Er_{B_{iy}}$	${}^Er_{B_{iz}}$
Cable 1	0	0	1	-0.15	-0.1	0.05
Cable 2	1	0	1	0.15	-0.1	0.05
Cable 3	1	1	1	0.15	0.1	0.05
Cable 4	0	1	1	-0.15	0.1	0.05
Cable 5	0.5	0	0	0	-0.1	-0.05
Cable 6	1	1	0	0.15	0.1	-0.05
Cable 7	0	1	0	-0.15	0.1	-0.05

To allow visualisation of the resulting workspace, the end effector is assumed to have constant orientation. The WCW of two orientations, $\alpha = \beta = \gamma = 0$, and $\alpha = \beta = 0, \gamma = 5^\circ$, will be presented. The bounds for the translational variables were selected to be $x, y, z \in [0, 1]$ m. The WCW will be determined analytically with respect to pose variable x, for varying values of y and z with step sizes of $\Delta y = \Delta z = 0.01$m.

5.2.1 Proposed Hybrid Analytical-Numerical Approach

It was shown in Section 4.1 that the selection of translational generalised variables would result in univariate cubic equations. In this simulation, x is selected and the remaining variables, y, z, α, β and γ are uniformly varied within the defined bounds as shown in Algorithm 2. The proposed approach provides a point-based measure along y, z, α, β and γ, while the WCC is satisfied continuously along $x_l < x < x_u$. Denoting the number of steps for the pose variables α, β, γ, x, y and z as a, b, c, d, e and f, respectively, the computational complexity of the proposed approach for non-constant orientation

WCW evaluation is $O(abcef)$, with the fundamental operation of solving for (21) at each iteration. Performing a similar analysis for the point-wise approach, the computational complexity is expected to be $O(abcdef)$, with the fundamental operation as the verification of the WCC from (13).

6 Results and Discussion

The α-β cross-sections of the WCW for the 3-DOF manipulator with $\Delta\alpha = \Delta\beta = \Delta\gamma = \frac{\pi}{60}$ rad at $\gamma \approx \frac{\pi}{6}$ rad for the proposed and point-wise approaches are shown in Figures 4(a) and 4(b), respectively. Additionally, the admitted workspace satisfying the WCC of each approach is demonstrated through lines and dots, respectively. From the cross-sections, it can be observed that two disconnected workspace volumes exist. Figure 5 shows the 3D visualisation of one of these volumes determined using each approach. The locality problem for both approaches have been disregarded for the purpose of visualisation.

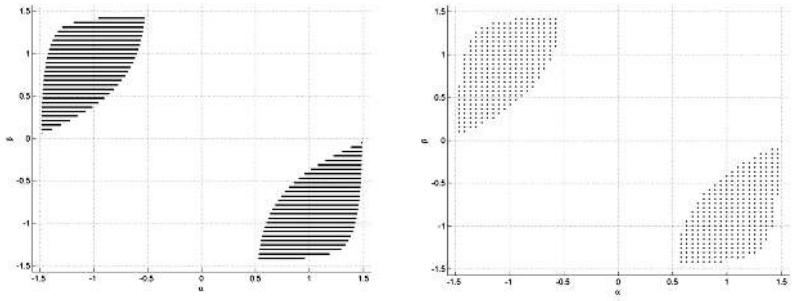

(a) Proposed approach (b) Point-wise approach

Fig. 4. α-β cross-section of the 3-DOF manipulator's WCW at $\gamma \approx \frac{\pi}{6}$ rad with $\Delta\alpha = \Delta\beta = \Delta\gamma = \frac{\pi}{60}$ rad for $\alpha, \beta \in \left[-\frac{\pi}{2}, \frac{\pi}{2}\right]$ rad

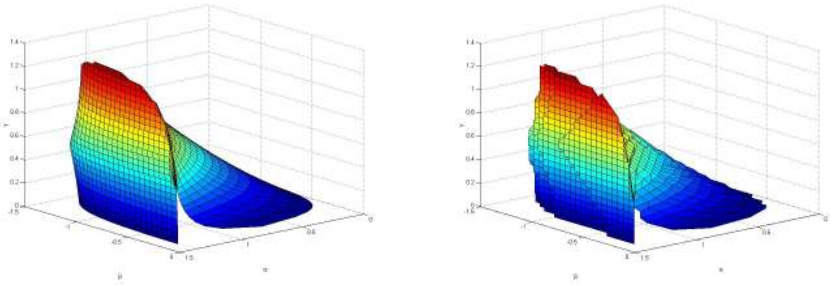

(a) Proposed approach (b) Point-wise approach

Fig. 5. 3-D Visualisation of the 3-DOF manipulator's workspace for $\alpha, \gamma \in [0, \frac{\pi}{2}]$ rad and $\beta \in [-\frac{\pi}{2}, 0]$ rad

Comparing the cross-sections and 3D representations of the two techniques, it can be observed that the proposed approach produces a more accurate definition of workspace contour, where as the artifacts of discretisation are more prominent in the point-wise approach. This can be observed when the region size and the step-size are of similar magnitude, where the point-wise evaluation lacks the resolution required to clearly depict the region. The consequence of this is the possibility in misinterpreting the workspace shape. The cross-section at $\gamma \approx \frac{3\pi}{8}$ rad in Figure 6 shows an example where the workspace shape determined by the point-wise approach is difficult to identify compared to the proposed method. This is further illustrated in the cross-section at $\gamma \approx \frac{7\pi}{16}$ rad in Figure 7, where the point-wise approach shows two smaller sections that appear to be disconnected. In contrast, the proposed approach clearly shows a single thin segment of workspace. Although the proposed approach produces solutions local to the β and γ values, the determined workspace boundaries and regions are the exact solutions of the WCW within numerical computational error. This produces a more accurate representation of the workspace geometry without any dependence on $\Delta\alpha$.

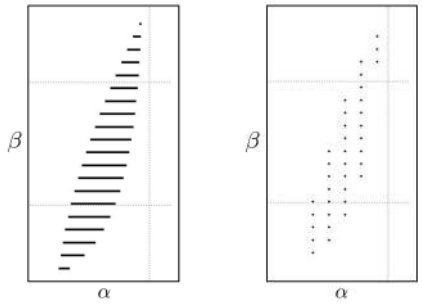

(a) Proposed approach (b) Point-wise approach

Fig. 6. α-β cross-section of the 3-DOF manipulator's workspace at $\gamma \approx \frac{3\pi}{8}$ rad with $\Delta\alpha = \Delta\beta = \Delta\gamma = \frac{\pi}{60}$ rad

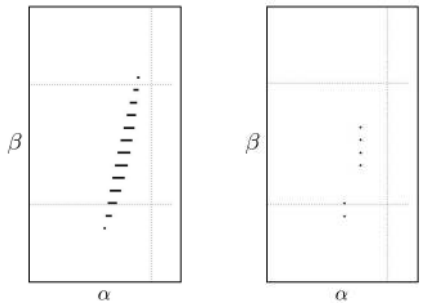

(a) Proposed approach (b) Point-wise approach

Fig. 7. α-β cross-section of the 3-DOF manipulator's workspace at $\gamma \approx \frac{7\pi}{16}$ rad with $\Delta\alpha = \Delta\beta = \Delta\gamma = \frac{\pi}{60}$ rad

The accuracy of the point-wise approach could be increased by using smaller step sizes $\Delta\alpha$, $\Delta\beta$ and $\Delta\gamma$. Figures 8 and 9 show the same cross-sections at $\gamma \approx \frac{3\pi}{8}$ rad and $\gamma \approx \frac{7\pi}{16}$ rad with a step-size of $\Delta\alpha = \Delta\beta = \Delta\gamma = \frac{\pi}{200}$ rad. With this step-size, it is apparent that the point-wise approach produces more accurate workspace representations compared to those shown in Figures 6(b) and 7(b). Despite the finer step-size, the discretisation around the workspace boundary is still visible. In comparison, the proposed approach provides more information between the gaps for β and γ, as shown in Figures 8(a) and 9(a), but has no effect on the accuracy of the solution with respect to α. These observations suggest that the proposed approach can be considered as equivalent to the point-wise approach with $\Delta\alpha = \varepsilon$, where ε is the numerical error involved in the computation of the polynomial roots. Observing the computational complexity for the point-wise evaluation approach, the increased number of steps in α will have a significant impact on its efficiency.

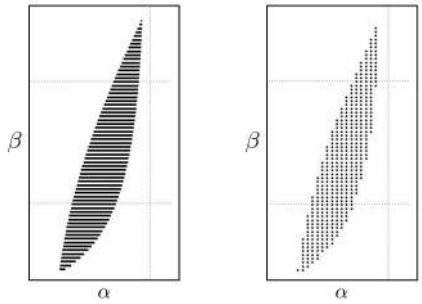

(a) Proposed approach (b) Point-wise approach

Fig. 8. α-β cross-section of the 3-DOF manipulator's workspace at $\gamma \approx \frac{3\pi}{8}$ rad with $\Delta\alpha = \Delta\beta = \Delta\gamma = \frac{\pi}{200}$ rad

To compare the approaches, two different scenarios to vary the step-sizes in workspace generation have been considered. In both cases, the time efficiency of each approach and the volume ratio from (36) have been measured for the setup described in Section 5.1.

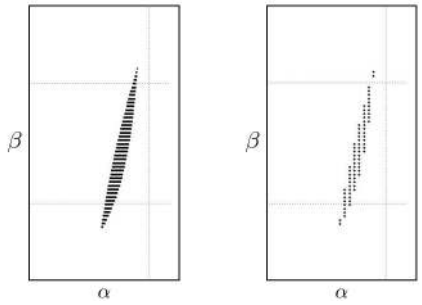

(a) Proposed approach (b) Point-wise approach

Fig. 9. α-β cross-section of the 3-DOF manipulator's workspace at $\gamma \approx \frac{7\pi}{16}$ rad with $\Delta\alpha = \Delta\beta = \Delta\gamma = \frac{\pi}{200}$ rad

Case 1 : Step-sizes of all pose variables are uniform, $\Delta\alpha = \Delta\beta = \Delta\gamma = \Delta x$, and varied between $\frac{\pi}{20}$ and $\frac{\pi}{200}$ rad. This is expected to be the more commonly used scenario when performing analysis on the workspace geometry and features.

Case 2 : Step-sizes of pose variables β and γ, $\Delta\beta$ and $\Delta\gamma$ are chosen as a constant value of $\Delta\beta = \Delta\gamma = \frac{\pi}{20}$ rad, while $\Delta\alpha$ is varied between $\frac{\pi}{20}$ and $\frac{\pi}{3200}$ rad. This allows a more direct comparison on the accuracy between the approaches for varying $\Delta\alpha$.

The results for case 1 are shown in Table 3, where it can be observed that the proposed approach has much lower computational times than the point-wise approach. Furthermore, this becomes increasingly significant for smaller step-sizes, conforming to the computational complexities determined previously. Denoting the number of steps in γ as c, derived from step-size Δx and bounds on γ, the commonly used point-wise approach has an algorithmic complexity of $O(c^3)$, while for the proposed approach it is $O(c^2)$. Despite having different fundamental operations in the complexity analysis, it appears that the numerical polynomial root solving is more efficient in comparison to multiple point-wise evaluations. In addition to the advantage in efficiency, the volume ratio shows that the proposed approach has a higher accuracy in workspace determination. With decreasing step-size, it can be observed that the volume ratio approaches unity, suggesting that the workspace region from the point-wise approach is converging to the proposed approach. It is important to note that the volume ratio is not an absolute measure of accuracy and is highly dependent on the workspace geometry for the particular cable configuration. Since the error in the point-wise approach occurs due to the discretisation of the workspace boundary by Δx, the magnitude of this error is dependent on the workspace's surface to volume ratio. Hence the volume ratio can only be used as an indication of accuracy for this cable configuration.

Table 3. Computational time and volume ratio for varying $\Delta\alpha = \Delta\beta = \Delta\gamma = \Delta x$

	Computational Time (sec)		
Δx (rad)	Proposed Approach	Point-wise Evaluation	V_r
$\pi/20$	1.0608	4.6176	0.7217
$\pi/40$	3.2292	33.9146	0.8458
$\pi/60$	6.8328	109.7311	0.9067
$\pi/80$	11.9185	258.0569	0.9280
$\pi/100$	18.5797	507.9081	0.9430
$\pi/200$	73.4453	3973	0.9720

Table 4 shows the computational time and volume ratio for case 2, where $\Delta\alpha$ is varied for constant β and γ. The computational complexity of the proposed and point-wise approaches are constant, $O(1)$, and linear, $O(a)$, respectively, where a represents the number of steps in the iteration of α as defined in Section 5.1.1. The constant computational complexity for the proposed approach is expected as there is no dependency on $\Delta\alpha$. Similar to the case with uniformly varying step-size, a decrease in step-size shows a convergence of the volume ratio towards unity. The results suggest that the proposed approach has the accuracy of the point-wise approach with $\Delta\alpha = \varepsilon \ll \frac{\pi}{3200}$.

Although comparable accuracy can be achieved using the point-wise approach with an extremely small step-size, it is apparent that the efficiency is significantly impacted. In addition, the interval-based satisfaction of the WCC of the

Table 4. Computational time and volume ratio for varying $\Delta\alpha$ with $\Delta\beta = \Delta\gamma = \frac{\pi}{20}$ rad

	Computational Time (sec)		
$\Delta\alpha$ (rad)	Proposed Approach	Point-wise Evaluation	V_r
$\pi/20$	1.0608	4.6176	0.7217
$\pi/50$	1.1076	11.2633	0.8860
$\pi/100$	1.0920	21.8401	0.9405
$\pi/200$	1.0452	42.9939	0.9704
$\pi/400$	1.1232	85.5821	0.9850
$\pi/800$	1.0843	171.3359	0.9920
$\pi/1600$	1.2012	336.2602	0.9960
$\pi/3200$	1.1700	673.2379	0.9980

proposed approach is desirable over the point-based locality of the point-wise approach, since the condition is satisfied for all continuous values along α within the lower and upper bounds (α_l, α_u). It should be noted that in achieving these advantages, the proposed approach requires explicit determination of the polynomials p_j and d in (29) from J^T, which are different depending on the manipulator topology. In comparison, the WCC condition in (13) can be utilised for the point-wise approach once J^T has been determined, regardless of manipulator topology.

Similarly, for the 6-DOF manipulator, the proposed algorithm was implemented to generate the *x*-*y* cross sections of the WCW for two constant orientations, $\alpha = \beta = \gamma = 0$, and $\alpha = \beta = 0, \gamma = 5^\circ$ for varying z values, as shown in Figures 10 and 11, respectively. Advantages of the proposed algorithm are similarly observed in this 6-DOF case, such as: the accurate determination of the WCW without any discretisation in the x dimension and the reduction of one exponential order in the expected computational time compared to the point-wise approach. The resulting workspace can be compared to the results of [21], and was observed to display similar symmetry and asymmetry in the admitted workspace, as shown in Figures 10 and 11, respectively. The asymmetry is introduced by the non-zero γ constant orientation.

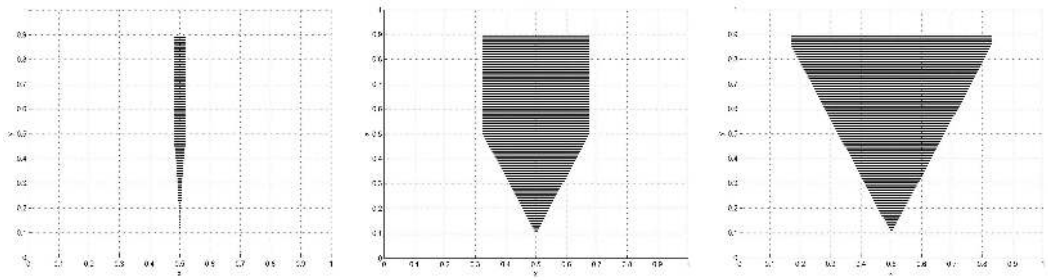

(a) $z = 0.1$ (b) $z = 0.5$ (c) $z = 0.9$

Fig. 10. *x*-*y* cross-section of 6-DOF manipulator's WCW at $\alpha = \beta = \gamma = 0^\circ$ with $\Delta y = 0.01$ m for $x, y \in [0, 1]$ m

The proposed approach can be regarded as a hybrid of numerical and analytical techniques, where the analytical form of the workspace region is solved with respect to a single variable, and the remaining pose variables are iteratively varied in the evaluation of the WCW within the region of interest, as discussed in Section 4. As a result, the level of accuracy known from the purely analytical techniques is maintained while significantly reducing its algebraic complexity.

7 Conclusions

A hybrid approach utilising analytical formulations within conventional numerical methods for a completely restrained cable driven manipulator was presented. It was shown that despite the complexity, the algebraic inequalities defining the WCW can be simplified to a set of univariate polynomial inequalities by considering a single variable for analysis. The complexities of the polynomial inequalities were determined for a general spatial manipulator and a 3-DOF manipulator. It

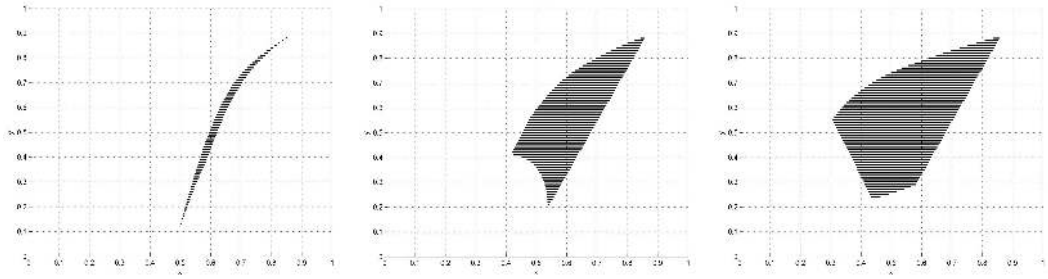

(a) $z = 0.1$ (b) $z = 0.5$ (c) $z = 0.9$

Fig. 11. x-y cross-section of 6-DOF manipulator's WCW at $\alpha = \beta = 0^\circ, \gamma = 5^\circ$ with $\Delta y = 0.01$ m for $x, y \in [0, 1]$ m

was shown that this approach is significantly more efficient compared to exhaustive numerical search techniques that evaluate in a point-wise manner. Efficient generation and evaluation of workspace provided by the proposed WCW determination approach allows the potential of comparing and optimising cable arrangements in an automated manner. Future work will focus on utilising the proposed technique in determining other types of cable driven parallel manipulator workspace, and to apply these in the optimisation of cable configurations given the desired workspace characteristics.

References

[1] Merlet, J.-P., 2000. *Parallel Robots*. Kluwer, Dordrecht.

[2] Albus, J. S., Bostelman, R. V., and Dagalakis, N., 1993. "The NIST robocrane". *J. Rob. Sys.,* **10**(5), pp. 709–724.

[3] Kawamura, S., Choe, W., Tanaka, S., and Pandian, S. R., 1995. "Development of an ultrahigh speed robot FALCON using wire drive system". In Proc. IEEE Int. Conf. Rob. Autom., pp. 215–220.

[4] Oh, S.-R., Mankala, K., Agrawal, S. K., and Albus, J. S., 2005. "A dual-stage planar cable robot: Dynamic modelling and design of a robust controller with positive inputs". *J. Mech. Des.,* **127**, pp. 612–620.

[5] Borgstrom, P. H., Borgstrom, N. P., Stealey, M. J., Jordan, B., Sukhatme, G. S., Batalin, M. A., and Kaiser, W. J., 2009. "Design and implementation of NIMS3D, a 3-d cabled robot for actuated sensing applications". *IEEE Trans. Rob.,* **25**(2), pp. 325–339.

[6] Williams II, R. L., Albus, J. S., and Bostelman, R. V., 2004. "3d cable-based cartesian metrology system". *J. Rob. Sys.,* **21**(5), pp. 237–257.

[7] Ferlay, F., and Gosselin, F., 2008. "A new cable-actuated haptic interface design". In Proc. Int. Conf. on Haptics: Perception, Devices and Scenarios, pp. 474–483.

[8] Bosscher, P., Williams II, R. L., Bryson, L. S., and Castro-Lacouture, D., 2007. "Cable-suspended robotic contour crafting system". *Autom. Constr.,* **17**, pp. 45–55.

[9] Surdilovic, D., and Bernhardt, R., 2004. "STRING-MAN: A new wire robot for gait rehabilitation". In Proc. IEEE Int. Conf. Rob. Autom., pp. 2031–2036.

[10] Mayhew, D., Bachrach, B., Rymer, W. Z., and Beer, R. F., 2005. "Development of the MACARM - a novel cable robot for upper limb neurorehabilitation". In Proc. IEEE Int. Conf. Rehab. Rob., pp. 299–302.

[11] Yang, G., Lin, W., Kurbanhusen, M. S., Pham, C. B., and Yeo, S. H., 2005. "Kinematic design of a 7-DOF cable-driven humanoid arm: a solution-in-nature approach". In Proc. IEEE/ASME Int. Conf. Adv. Int. Mechat., pp. 444–449.

[12] Agrawal, S. K., Dubey, V. N., Gangloff, Jr., J. J., Brackbill, E., Mao, Y., and Sangwan, V., 2009. "Design and optimization of a cable driven upper arm exoskeleton". *J. Med. Dev.,* **3**, p. 031004.

[13] Valero, F., Mata, V., and Besa, A., 2006. "Trajectory planning in workspaces with obstacles taking into account the dynamic robot behaviour". *Mech. Mach. Theory,* **41**, pp. 525–536.

[14] Perreault, S., and Gosselin, C. M., 2008. "Cable-driven parallel mechanisms: Application to a locomotion interface". *J. Mech. Des.,* **130**, p. 102301.

[15] Oh, S.-R., and Agrawal, S. K., 2005. "Cable suspended planar robots with redundant cables: Controllers with positive tension". *IEEE Trans. Rob.,* **21**(3), pp. 457–464.

[16] Pusey, J., Fattah, A., Agrawal, S., and Messina, E., 2004. "Design and workspace analysis of a 6-6 cable-suspended parallel robot". *Mech. Mach. Theory,* **39**, pp. 761–778.

[17] Barrette, G., and Gosselin, C. M., 2005. "Determination of the dynamic workspace of cable-driven planar parallel mechanisms". *J. Mech. Des.,* **127**, pp. 242–248.

[18] Gouttefarde, M., Merlet, J.-P., and Daney, D., 2007. "Wrench-feasible workspace of parallel cable-driven mechanisms". In Proc. IEEE Int. Conf. Rob. Autom., pp. 1492–1497.

[19] Bosscher, P., Riechel, A. T., and Ebert-Uphoff, I., 2006. "Wrench-feasible workspace generation for cable-driven robots". *IEEE Trans. Rob.,* **22**(5), pp. 890–902.

[20] Pham, C. B., Yeo, S. H., Yang, G., and Chen, I.-M., 2009. "Workspace analysis of fully restrained cable-driven manipulators". *Rob. and Auton. Sys.,* **57**, pp. 901–912.

[21] Pham, C. B., Yeo, S. H., Yang, G., Kurbanhusen, M. S., and Chen, I.-M., 2006. "Force-closure workspace analysis of cable-driven parallel mechanisms". *Mech. Mach. Theory,* **41**, pp. 53–69.

[22] Diao, X., and Ma, O., 2007. "A method of verifying force-closure condition for general cable manipulators with seven cables". *Mech. Mach. Theory,* **42**, pp. 1563–1576.

[23] Gouttefarde, M., and Gosselin, C. M., 2006. "Analysis of the wrench-closure workspace of planar parallel cable-driven mechanisms". *IEEE Trans. Rob.,* **22**(3), pp. 434–445.

[24] Stump, E., and Kumar, V., 2006. "Workspaces of cable-actuated parallel manipulators". *J. Mech. Des.,* **128**, pp. 159–167.

[25] Williams II, R. L., and Gallina, P., 2002. "Planar cable-direct-driven robots: Design for wrench exertion". *J. Int. Rob. Sys.,* **35**, pp. 203–219.

[26] Aref, M. M., and Taghirad, H. D., 2008. "Geometrical workspace analysis of a cable-driven redundant parallel manipulator: KNTU CDRPM". In Proc. IEEE/RSJ Int. Conf. Int. Rob. Sys., pp. 1958–1963.

[27] Ming, A., and Higuchi, T., 1994. "Study on multiple degrees-of-freedom positioning mechanism using wires (part 1) - concept, design and control". *Int. J. Japan Social Eng.,* **28**(2), pp. 131–138.